

The Eclipsing Binary BG Geminorum: Improved Constraints on the Orbit and the Structure of the Accretion Disk

Scott J. Kenyon, Paul J. Groot¹

Smithsonian Astrophysical Observatory, 60 Garden Street, Cambridge, MA 02138

and

Priscilla Benson

Wellesley College, Whitin Observatory, 106 Central Street, Wellesley, MA 02181-8286

ABSTRACT

We describe new optical photometric and spectroscopic observations of the semi-detached eclipsing binary BG Geminorum. A large change in the amount of Mg I absorption at secondary maximum indicates the presence of cool material in the outer edge of the disk surrounding the unseen primary star. Detection of weak He I emission implies a hot radiation source at the inner edge of the disk. If the velocity variations in the $H\beta$ emission line track the orbital motion of the primary star, the primary star has an orbital semi-amplitude of $K_1 = K_{H\beta} = 16.0 \pm 4.6 \text{ km s}^{-1}$. This result yields a mass ratio, $q = 0.22 \pm 0.07$, consistent with the $q = 0.1$ derived from the large ellipsoidal variation. Despite this progress, the nature of the primary star – B-type star or black hole – remains uncertain.

Subject headings: binaries: eclipsing – binaries: spectroscopic – stars: emission-line – stars: evolution – stars: individual (BG Gem)

1. INTRODUCTION

BG Geminorum was discovered by Hoffmeister (1933) and Jensch (1938) as a possible RV Tau star with an uncertain period of ~ 60 days. With a photographic magnitude of ~ 14 , the star languished in the General Catalog of Variable Stars (Kholopov 1985) until 1992, when Benson et al. (2000) discovered an ellipsoidal variation with an optical amplitude of ~ 0.5 mag and a period of 91.645 days. Light curves derived from optical spectrophotometry reveal a deep primary eclipse at short wavelengths, $\lambda \lesssim 4400 \text{ \AA}$, and a shallow secondary eclipse at longer wavelengths.

¹present address: Department of Astrophysics, University of Nijmegen, P.O. Box 9010, 6500 GL Nijmegen, The Netherlands

The ellipsoidal light curve and the radial velocity curve of the K0 I secondary star indicate a semi-detached binary, where the K0 star transfers material into an accretion disk around an unseen primary star. The primary star is either an early B-type star or a black hole (Benson et al. 2000).

This paper reports new optical and spectroscopic observations of BG Gem. These data yield an orbit for H β emission from the disk. Coupled with an improved ephemeris and orbit for the K0 secondary, this result indicates a mass ratio, $q \equiv M_{K0}/M_1 = 0.22 \pm 0.07$, where M_1 is the mass of the primary star and M_{K0} is the mass of the secondary star. This result is consistent with the $q \approx 0.1$ derived from the optical light curve. The observations also provide additional information on the structure of the disk. A significant increase in Mg I absorption at secondary minimum shows that the outer part of the disk is cool, with $T \sim 4000$ K at $R \approx 0.26$ AU from the primary star. Despite the detection of weak He I emission lines, the nature of the central ionizing source is uncertain. The absolute H I and He I line fluxes appear to rule out a B-type primary star as the ionizing source and may indicate radiation from a boundary layer at the inner edge of the disk.

We begin with a summary of the observations in §2, continue with the analysis in §3, and conclude with a brief discussion in §4.

2. OBSERVATIONS

Student observers acquired optical photometry of BG Gem with standard VR_CI_C filters and a Photometrics PM512 camera mounted on the Wellesley College 0.6-m Sawyer telescope. Benson et al. (2000) describe the instrument and the data reduction. Because Wellesley is not a photometric site, we derive photometry of BG Gem relative to two comparison stars. The relative photometry has 1σ probable errors of ± 0.011 mag at V, ± 0.014 mag at R_C, and ± 0.011 mag at I_C (Benson et al. 2000). Table 1 lists new relative photometry of BG Gem and a comparison star as a function of time (the Heliocentric Julian Date, JD) and photometric phase (ϕ). These new data yield an improved ephemeris for primary minimum and photometric phase,

$$\text{Min} = \text{JD } 2449088.96 \pm 0.94 + (91.60 \pm 0.55) \cdot E . \quad (1)$$

P. Berlind, M. Calkins, and several other observers acquired low resolution optical spectra of BG Gem with FAST, a high throughput, slit spectrograph mounted at the Fred L. Whipple Observatory 1.5-m telescope on Mount Hopkins, Arizona (Fabricant *et al.* 1998). They used a 300 g mm^{-1} grating blazed at 4750 \AA , a $3''$ slit, and a thinned Loral 512×2688 CCD. These spectra cover $3800\text{--}7500 \text{ \AA}$ at a resolution of 6 \AA . We wavelength-calibrate the spectra in NOAO IRAF². After trimming the CCD frames at each end of the slit, we correct for the bias level, flat-field each frame, apply an illumination correction, and derive a full wavelength solution from calibration

²IRAF is distributed by the National Optical Astronomy Observatory, which is operated by the Association of Universities for Research in Astronomy, Inc. under contract to the National Science Foundation.

lamps acquired immediately after each exposure. The wavelength solution for each frame has a probable error of $\pm 0.5 \text{ \AA}$ or better. To construct final 1-D spectra, we extract object and sky spectra using the optimal extraction algorithm APEXTRACT within IRAF. Most of the resulting spectra have moderate signal-to-noise, $S/N \gtrsim 30$ per pixel.

We derive radial velocities from the strong absorption and emission lines on FAST spectra. For absorption line velocities, we cross-correlate the FAST spectra against the best-exposed spectrum, where the velocity is set by cross-correlation against standard stars with known velocities (see Tonry & Davis 1979; Kurtz & Mink 1998). To avoid contamination from the hot primary, we restrict the cross-correlation to $\lambda\lambda 5000\text{--}6800$. We measure emission line velocities from cross-correlations with an emission-line template, as described by Kurtz & Mink (1998). We adopt the velocity of $H\beta$ as the emission line velocity, because $H\alpha$ may be blended with [N II] emission on our low resolution spectra. We estimate errors of $\pm 30 \text{ km s}^{-1}$ for absorption lines and $\pm 40 \text{ km s}^{-1}$ for emission lines (see also Kurtz & Mink 1998). Table 2 contains the first ten radial velocity measurements. The third column lists the measured absorption velocities as a function of JD and ϕ ; the fourth column lists measurements for $H\beta$. The electronic version of this paper includes all 189 radial velocity measurements.

To analyze the phase variations of the absorption and emission line spectra, we measure continuum magnitudes and indices using narrow passbands (O’Connell 1973; Worthey 1994). Table 3 of Benson et al. (2000) lists the central wavelength λ and width $\delta\lambda$ for each. The absorption and emission indices, derived using SBANDS within IRAF, are $I_\lambda = -2.5 \log(F_\lambda/\bar{F})$, where F_λ is the average flux in the passband λ and \bar{F} is the continuum flux interpolated between the fluxes in the neighboring blue band centered at λ_b and the red band centered at λ_r . Table 3 lists the first ten measured indices along with emission line equivalent widths as a function of JD and ϕ . The electronic version of this paper contains all 191 measurements of absorption indices and emission line equivalent widths.

To search for weak high ionization emission lines in BG Gem, we examine coadded spectra. We construct spectra in 20 phase bins with width $\Delta\phi = 0.05$ at integral multiples of $\phi = 0.05$. The spectra provide fair detections of He I $\lambda 4471$ and $\lambda 5876$ at most orbital phases with equivalent widths of $0.5 \pm 0.2 \text{ \AA}$. The lines disappear at primary eclipse. These data provide no evidence for higher ionization features such as He II $\lambda 4686$. The coadded spectra suggest a weak broad pedestal of $H\alpha$ and $H\beta$ emission with a velocity width of $\sim 4000 \text{ km s}^{-1}$. At low resolution, these features are difficult to disentangle from numerous K-type absorption features and may not be real.

3. ANALYSIS

3.1. Radial Velocities

The absorption line radial velocities show clear evidence for orbital motion correlated with the photometric phase (Figure 1). We analyze these observations using the Monet (1979) Fourier transform algorithm (see also Kenyon & Garcia 1986). The best spectroscopic period, $P_{spec} = 91.61 \pm 2.53$ days, agrees with the photometric period. A circular orbit with $P = P_{phot}$ from equation (1) fits the orbit well. This solution has an orbital semi-amplitude, $K_{K0} = 71.7 \pm 3.4$ km s⁻¹, and a fractional semi-major axis, $A_{K0} \sin i = 0.60 \pm 0.03$ AU. Spectroscopic conjunctions occur 0.69 days prior to photometric minima, with

$$\text{Conj} = \text{JD } 2451012.28 \pm 0.71 + 91.60 \cdot E . \quad (2)$$

The phase difference between primary eclipses and spectroscopic conjunctions has a significance of 1σ . The mass function is $M_1^3 \sin^3 i = (3.5 \pm 0.5) M_\odot (M_1 + M_{K0})^2$. If $\sin i = 1$, this result becomes $M_1 \approx 3.5 M_\odot (1 + q)^2$, where $q \equiv M_{K0}/M_1$ is the mass ratio. The eclipses place an upper limit on the mass of the primary star. For $i \gtrsim 65^\circ$, $M_1 \lesssim 5.7 M_\odot$ for $q = 0.1$ and $M_1 \lesssim 7 M_\odot$ for $q = 0.2$.

Solutions with eccentric orbits may improve the fit to the data. Iterations in Fourier and configuration space yield $e = 0.09 \pm 0.03$. The Lucy & Sweeney (1971) test suggests that the non-zero e is marginally significant. We derive Lucy-Sweeney probabilities of $p_{LS} = 3.6\%$ for the Fourier solution and $p_{LS} = 4.9\%$ for the configuration space solution; $p_{LS} < 5\%$ implies the eccentricity is non-zero with 95% confidence. Radial velocity measurements using higher resolution spectra could resolve this ambiguity. In this paper, we adopt the circular solution with the parameters quoted above. If the K0 I secondary has negligible mass and $\sin i = 1$, these results place a lower limit on the mass of the primary, $M_1 \gtrsim 3.5 M_\odot$.

Radial velocities of the H β emission line also vary with photometric phase (Figure 2). The line variations during primary minimum are consistent with the eclipse of a rapidly rotating disk, where the blue-shifted half of the disk is eclipsed first during ingress and is revealed first during egress. The velocity variations of H β outside primary minimum provide a direct estimate of the mass ratio. The best-fitting circular orbit to data with $\phi = 0.05$ – 0.95 has an orbital semi-amplitude, $K_{H\beta} = 16.0 \pm 4.6$ km s⁻¹ and a fractional semi-major axis, $A_{H\beta} \sin i = 0.13 \pm 0.04$. The orbital conjunction derived from the H β velocities, $\text{Conj}(\text{H}\beta) = \text{JD } 2451009.65 \pm 4.6$, is 2.91 days prior to primary eclipse and is 2.63 days prior to the spectroscopic conjunction defined by the absorption line velocities. Together with the absorption line orbit, these results indicate that the H β line provides a reasonable first estimate for the orbit of the disk surrounding the primary star. If the orbital semi-amplitude of the unseen primary is 16.0 km s⁻¹, the mass ratio is $q = 0.22 \pm 0.07$. For $\sin i \approx 1$, the component masses are then $M_1 = 4.3 \pm 0.8 M_\odot$ and $M_{K0} = 0.95 \pm 0.45 M_\odot$. These results are consistent with the $q \approx 0.1$ derived from the ellipsoidal light curve (Benson et al. 2000).

3.2. Mg I Absorption from the Disk

Most of the low excitation absorption lines in BG Gem spectra provide a good measure of the spectral type for the K-type secondary star (Benson et al. 2000). The Ba I blend at 6495 Å is constant with photometric phase (Figure 3). Absorption lines at shorter wavelengths vary consistently with photometric phase (Figure 3; Benson et al. 2000). All lines grow stronger at $\phi = 0$, when the K-type star eclipses light from the primary. The absorption line strengths at primary minimum are consistent with a K0 I spectral type for the secondary star (Benson et al. 2000).

The equivalent widths of several absorption lines rise at $\phi \approx 0.5$, when the disk surrounding the primary eclipses the secondary star. The Na I, Mg I, and several other low ionization lines are as strong at secondary minimum as at primary minimum (Figure 3). The disk surrounding the primary star is the only possible source of this extra absorption. The duration of the second maximum in Mg I line strength yields a reliable estimate for the sum of the radius of the K0 I secondary and the radius of the region that produces Mg I absorption, $R_{K0\ I} + R_{Mg\ I} \approx (0.60 \pm 0.03)$ A; this yields $R_{K0\ I} + R_{Mg\ I} \approx 0.44$ AU for $A = 0.73$ AU. With $R_{K0\ I} \approx 0.18$ AU (Benson et al. 2000), the size of the Mg I region is then $R_{Mg\ I} \approx 0.26$ AU. This radius is larger than the $R_{H\alpha} \approx 0.22$ AU derived from the emission line eclipses (Benson et al. 2000).

The Mg I line strength appears to drop rapidly at $\phi = 0.5$, when our line-of-sight passes through the center of the primary and the surrounding accretion disk. The line strength recovers at $\phi = 0.51$ and then falls gradually as the system approaches orbital quadrature. Although our phase coverage at $\phi = 0.5$ is not superb, this behavior repeats over several eclipses.

We propose a simple explanation for the behavior of Mg I absorption at $\phi = 0.45$ – 0.55 . Because Mg I has an ionization potential of 7.6 eV, Mg is ionized to Mg II in the inner region of the disk that produces H α emission. If the outer part of the disk is cool, $T \sim 4000$ K, most Mg atoms are neutral and can absorb radiation from the K0 I secondary. We see this absorption at secondary minima when the K0 star lies behind the disk. The drop in Mg I absorption at $\phi = 0.5$ implies a ring geometry for Mg I atoms. The central hole of the ring, where magnesium is Mg II, yields a longer path length through the edge of the ring than through the center.

If the outer disk is heated by the central star, the Mg I absorption places some useful limits on the temperature of the central star. In most heating models, the disk temperature varies with radius as $T_d \propto R^{-n}$ with $n \approx \frac{1}{2}$ to $\frac{3}{4}$ (Kenyon & Hartmann 1987). With $T_d \approx 4000$ K at $R \approx 0.26$ AU, the limits on the temperature of the 4–5 M_\odot main sequence star are reasonable, $T_\star \sim 12,000$ K to 20,000 K.

3.3. He I Emission

We detect modest He I emission on coadded spectra of BG Gem. The $\lambda 5876$ line is blended with strong Na I D absorption lines and is difficult to measure accurately. The $\lambda 4471$ line has an

equivalent width of $\sim 0.5 \text{ \AA}$ at orbital quadratures and $\sim 1 \text{ \AA}$ at $\phi = 0.5$. Both lines disappear at primary eclipse. The integrated line flux is $F_{4471} \approx 7 \times 10^{-14} \text{ erg cm}^{-2} \text{ s}^{-1}$ for a visual reddening $A_V = 1.65 \text{ mag}$ (Benson et al. 2000). The total $\lambda 4471$ luminosity is $L_{4471} \approx 5 \times 10^{31} \text{ erg s}^{-1} (\text{d}/2.5 \text{ kpc})^2$. The He I $\lambda 5876$ luminosity is roughly a factor of two larger, but is more uncertain due to blending with Na I D. No other obvious He I or He II lines are visible on the coadded spectra.

Detection of He I emission implies a luminous source of high energy photons. For case B recombination, the observed $F_{4471}/F_{H\beta}$ intensity ratio requires an ionizing source with an effective temperature $T_{eff} \approx 25,000 \text{ K}$ (Osterbrock 1988). If the atmosphere of the primary star produces these photons, the observed H β and He I $\lambda 4471$ fluxes imply a B1–B2 V star with $L_1 \sim 5000 L_\odot$ (Spitzer 1978; Shaerer & de Koter 1997). Normal B1–B2 V stars have masses of 15–20 M_\odot (e.g., Vacca, Garmany, & Shull 1996; Shaerer & de Koter 1997, and references therein). These results are not consistent with a 4 M_\odot B5 main sequence star with $L \approx 1000 L_\odot$. The line fluxes thus preclude photoionization from a normal B-type star.

The dynamical mass and emission line fluxes are also inconsistent with a Be-type primary star. Known Be stars with He I emission have B1–B2 or earlier spectral types; Be stars with B4–B6 spectral types have weak He I absorption lines (Jaschek & Jaschek 1987). Known Be stars have very steep Balmer decrements indicative of optically thick H α ; H δ , H ϵ , and higher level transitions in the series are almost always strong absorption lines (Jaschek & Jaschek 1987; Torrejón et al. 1997). We detect H8 and H9 emission in BG Gem; the line fluxes are consistent with case B recombination for $A_V = 1.65 \text{ mag}$ (Benson et al. 2000). Be-type stars with strong H α emission also have large near-IR excesses from dusty circumstellar material (Dougherty et al. 1994). Near-IR photometry demonstrates that BG Gem has no substantial near-IR excess (Benson et al. 2000). Thus, the primary star in BG Gem is not a normal Be-type star.

Accretion provides another energy source for the H I and He I emission. The double-peaked H α and H β lines form in the disk surrounding the primary star. The inner part of this disk produces blue continuum emission which dominates the spectrum for $\lambda \lesssim 4500 \text{ \AA}$. There are two possible sources of high energy photons, the inner disk and the boundary layer between the inner disk and the stellar photosphere. If the inner disk has a temperature of $\sim 25,000 \text{ K}$, the boundary layer temperature should exceed $T_{bl} \sim 10^5 \text{ K}$ (Lynden-Bell & Pringle 1974; Kenyon & Webbink 1984). The lack of high ionization emission lines – as observed in some symbiotic stars (Kenyon & Webbink 1984; Kenyon *et al.* 1991) – precludes such a hot boundary layer. If instead the boundary layer alone is responsible for the He I emission, the radius of the central star is roughly (Kenyon *et al.* 1991)

$$R_1 \approx 5.5 R_\odot \left(\frac{L_{bl}}{1000 L_\odot} \right)^{0.4} \left(\frac{T_{bl}}{25,000 \text{ K}} \right)^{-1.8}. \quad (3)$$

For a boundary layer which radiates as a star with $T_{bl} = 25,000 \text{ K}$, the boundary layer luminosity is $L_{bl} \approx 3000 L_\odot$. The stellar radius is $R_1 \approx 8.5 R_\odot$. This solution implies an evolved primary star with $L_1 \approx 3500 L_\odot$, $T_{eff} \approx 15,000 \text{ K}$, and a dynamical mass of $\sim 4 M_\odot$. These properties are consistent with those derived from Mg I absorption lines produced in the outer disk. Because

we do not detect optical spectral features from this star, this solution is viable only if the outer edge of the disk hides the star from view. The accretion rate in this interpretation is large, $\dot{M} \approx 4\text{--}5 \times 10^{-4} M_{\odot} \text{ yr}^{-1}$. This large accretion rate implies very bright optical emission from the disk (Kenyon & Webbink 1984) which is inconsistent with the optical spectrum of BG Gem unless $i \gtrsim 86^{\circ}$.

4. DISCUSSION AND SUMMARY

Our new optical spectra yield a better understanding of the orbit, geometry, and disk structure in BG Gem. Absorption line radial velocities derived from these spectra reduce the uncertainties in the orbital parameters by $\sim 25\%$ and confirm that the minimum mass for the primary star is $3.5\text{--}4.0 M_{\odot}$. Using the $H\beta$ emission line, we also derive a tentative orbit for the disk surrounding the primary star. Although the interpretation of orbits derived from material in a disk is controversial (e.g., Warner 1995), the mass ratio $q \approx 0.2$ inferred from this orbit is consistent with the $q \approx 0.1$ derived from the optical light curve (Benson et al. 2000). The velocity amplitude of $K_{H\beta} = 16.0 \pm 4.6 \text{ km s}^{-1}$ is at the limit of our FAST spectra; improvements in this measurement require higher resolution spectra.

The behavior of Mg I and other neutral absorption lines at $\phi \approx 0.5$ implies a cool ring of material in the outer disk with $T \sim 4000 \text{ K}$. The outer radius of this ring, $\sim 0.26 \text{ AU}$, is slightly larger than the radius of the ionized region that produces H I emission. The outer radius of the Mg I ring is $\sim 70\%$ of the radius of the Roche lobe of the primary star, well within the boundary where tidal forces truncate the disk.

The detection of weak He I emission implies a modest source of high energy photons from the primary star, the inner disk, or the boundary layer between the inner disk and the primary star. The ratio of the He I $\lambda 4471$ flux to the $H\beta$ flux implies a temperature of $\sim 25,000 \text{ K}$ for the ionizing source. If the disk does not occult any of the ionized H II region, the luminosity of the ionizing source is $\sim 1000\text{--}5000 L_{\odot}$. If the primary is a B-type star, the dynamical mass estimates favor a B4–B6 giant which lies hidden behind the outer edge of the accretion disk. For an orbital inclination $i \approx 85^{\circ}$, this picture implies a disk luminosity which exceeds the observed disk luminosity. If the orbital inclination is larger than 85° , the outer disk probably hides some of the He I and other moderate ionization emission lines from our line-of-sight. In this case, we cannot make a meaningful derivation of the physical properties of the primary star.

Our data do not rule out the possibility that the primary star is a black hole (Benson et al. 2000). Although we do not detect X-rays or high ionization emission lines – such as the He II features observed in other black hole binaries – the outer edge of the disk can hide these features from our line-of-sight for $i \gtrsim 85^{\circ}$ (Benson et al. 2000). Our coadded spectra provide weak evidence for $H\alpha$ emission with velocities of $\sim 2000 \text{ km s}^{-1}$. The maximum rotational velocity for material in a disk surrounding a B-type star is $\sim 700 \text{ km s}^{-1}$. If confirmed with higher resolution optical

spectra, high velocity H α emission would preclude a B-type primary star and favor a black hole primary star in BG Gem.

Making further progress on this system requires ultraviolet spectra and more intensive analysis of the optical spectra. We have an approved program with the *Hubble Space Telescope* to acquire low resolution ultraviolet spectra at specific orbital phases. Detection of a strong ultraviolet continuum or ultraviolet absorption lines from Si II and Si III (among others) would indicate a B-type primary; failure to detect these features or detection of (broad) high ionization emission lines would favor a black hole primary. Optical spectra acquired during primary eclipse provide an opportunity to use maximum entropy techniques to construct the surface brightness profile and eclipse maps of the accretion disk surrounding the primary star (e.g., Horne 1985; Marsh & Horne 1988; Warner 1995; Groot et al. 2001; Diaz 2001). The cycle-to-cycle stability of BG Gem (see Figure 4) should yield good disk ‘images’ to test for the presence of high velocity material in the disk and to search for the source of high energy photons at the inner disk. These techniques might also clarify the geometry of Mg I absorption in the outer disk. We plan to address these issues in future papers.

We thank P. Berlind, M. Calkins, and other queue observers at the FLWO 60'' telescope for acquiring the FAST spectra used in this project. Susan Tokarz made the preliminary reductions of the FAST spectra. PJG was supported by a CfA fellowship.

REFERENCES

- Benson, P., Dullighan, A., Bonanos, A., McLeod, K. K., & Kenyon, S. J. 2000, *AJ*, 119, 890
- Diaz, M. P. 2001, *ApJ*, 553, 177
- Dougherty, S. M., Waters, L. B. F. M., Burki, G., Cote, J., Cramer, N., van Kerkwijk, M. H., & Taylor, A. R. 1994, *A&A*, 290, 609
- Fabricant, D. G., Cheimets, P., Caldwell, N., & Geary, J. 1998, *PASP*, 110, 79
- Groot, P. J., Rutten, R. G. M., Van Paradijs, J., 2001, *A&A*, 368, 183
- Hoffmeister, C. 1933, *Sonn. Mitt* No. 22
- Horne, K. 1985, *MNRAS*, 213, 129
- Jaschek, C., & Jaschek, M. 1987, *The Classification of Stars*, Cambridge University Press, Cambridge
- Jensch, A. 1938, *KVBB* No. 19
- Kenyon, S. J., & Garcia, M. R. 1986, *AJ*, 91, 125

- Kenyon, S. J., & Hartmann, L. 1987, *ApJ*, 323, 714
- Kenyon, S. J., Oliverson, N. G., Mikołajewska, J., Mikołajewski, M., Stencel, R. E., Garcia, M. R., & Anderson, C. M. 1991, *AJ*, 101, 637
- Kenyon, S.J., & Webbink, R. F. 1984, *ApJ*, 279, 252
- Kholopov, P. N. ed. 1985, *General Catalog of Variable Stars* (4th ed.), Moscow: Nauka
- Kurtz, M. J., & Mink, D. J. 1998, *PASP*, 110, 934
- Lynden-Bell, D., & Pringle, J. E. 1974, *MNRAS*, 168, 603
- Lucy, L. B., & Sweeney, M. A. 1971, *AJ* 76, 544
- Marsh, T. R., & Horne, K. 1988, *MNRAS*, 235, 269
- Monet, D. G. 1979, *ApJ*, 234, 275
- O’Connell, R. W. 1973, *AJ*, 78, 1074
- Osterbrock, D. E. 1988, *The Astrophysics of Gaseous Nebulae and Active Galactic Nuclei*, University Science Books, Mill Valley, CA
- Shaerer, D., & de Koter, A. 1997, *A&A*, 322, 598
- Spitzer, L. 1978, *Physical Processes in the Interstellar Medium*, Wiley-Interscience, New York
- Tonry, J., & Davis, M. 1979, *AJ*, 84, 1511
- Torrejón, J. M., Fabregat, J., Bernabeu, G., & Alba, S. 1997, *A&AS*, 124, 329
- Vacca, W. D., Garmany, C. D., & Shull, J. M. 1996, *ApJ*, 460, 914
- Warner, B. 1995, *Cataclysmic Variable Stars*, Cambridge, Cambridge University Press
- Worthey, G. 1994, *ApJS*, 95, 107

Table 1. Optical Photometry

JD	Phase	$\delta V(\text{BG})$	$\delta V(\text{com})$	$\delta R_C(\text{BG})$	$\delta R_C(\text{com})$	$\delta I_C(\text{BG})$	$\delta I_C(\text{com})$
48728.5230	0.065	+0.200	+0.369
49059.5030	0.678	+0.291	1.079
50156.5270	0.655	+0.232	1.044
50168.4870	0.785	+0.190	+0.682
50500.5570	0.410
50851.5620	0.242	-0.202	+0.673
50911.5113	0.897	+0.343	+1.091	+0.146	+0.428	-0.057	+0.652
51215.5767	0.216	...	+1.067	-0.223	+0.382	...	+0.705
51276.5300	0.882	+0.122	+0.367	-0.102	+0.720
51577.5313	0.168	+0.158	+0.978	+0.003	+0.326	-0.151	+0.679
51580.5350	0.201	+0.025	+0.366
51590.6033	0.311	+0.171	+1.060	+0.007	+0.346	-0.160	+0.684
51592.6013	0.332	+0.220	+1.053	+0.077	+0.367	-0.126	+0.689
51604.6123	0.463	+0.734	+1.041	+0.563	+0.362	+0.431	+0.709
51609.5610	0.517	+0.408	+0.708
51613.5735	0.561	+0.213	+0.440	+0.227	+0.607
51627.6090	0.715	-0.244	+0.798
51952.6777	0.263	+0.098	+1.043	-0.042	+0.365	-0.264	+0.649
51953.5237	0.273	+0.050	+0.965	+0.048	+0.449	-0.156	+0.734
51954.5090	0.283	+0.129	+1.063	+0.028	+0.403
51958.6247	0.328	+0.199	+1.042	+0.043	+0.368	-0.143	+0.697
51959.5327	0.338	+0.216	+1.039	+0.042	+0.357	-0.106	+0.700
51962.6210	0.372	+0.260	+1.019	+0.123	+0.370	-0.053	+0.695
51967.5167	0.425	+0.582	+1.005	+0.398	+0.328	+0.059	+0.612
51968.5760	0.437	+0.482	+0.986	+0.236	+0.328
51993.5780	0.710	+0.174	+1.056	+0.006	+0.360	-0.175	+0.686
51996.5537	0.742	+0.180	+1.047	-0.045	+0.327	-0.207	+0.703
51997.5813	0.754	+0.149	+1.038	-0.020	+0.351	-0.193	+0.693
52004.6123	0.830	+0.201	+1.044	+0.038	+0.375	-0.141	+0.681
52005.5177	0.840	+0.236	+1.042	+0.083	+0.356	-0.109	+0.679

Table 2. Radial Velocities^a

JD	Phase	v_{abs}	$v_{H\beta}$
51547.8309	0.844	−16.790	+26.140
51547.8381	0.844	−12.160	+34.710
51550.8141	0.876	+11.680	+57.490
51552.7494	0.897	−36.480	−4.600
51552.7524	0.897	−42.240	−15.880
51555.8512	0.931	−29.990	−0.380
51557.7808	0.952	+32.920	+118.580
51571.6108	0.103	+43.590	+4.460
51571.6147	0.103	+39.510	+7.680
51572.7773	0.116	+58.040	+27.610

^aThe velocities are measured in km s^{−1}.

Table 3. Absorption and Emission Line Indices

JD	Phase	$I_{\text{Fe I}}$	$I_{\text{Mg I}}$	$I_{\text{Na I}}$	$I_{\text{Ba I}}$	$\text{EW}(H\beta)$	$\text{EW}(H\alpha)$
51547.8309	0.844	0.10	0.13	0.15	0.05	−8.900	−30.580
51547.8381	0.844	0.13	0.15	0.15	0.05	−10.270	−31.530
51550.8141	0.876	0.13	0.14	0.15	0.04	−10.090	−31.320
51552.7494	0.897	0.11	0.15	0.15	0.05	−9.560	−27.370
51552.7524	0.897	0.10	0.15	0.15	0.05	−6.320	−22.750
51555.8512	0.931	0.13	0.17	0.16	0.05	−9.270	−28.880
51557.7808	0.952	0.14	0.17	0.15	0.05	−9.260	−28.950
51571.6108	0.103	0.12	0.15	0.16	0.04	−9.120	−28.880
51571.6147	0.103	0.11	0.15	0.15	0.05	−9.200	−29.160
51572.7773	0.116	0.10	0.14	0.16	0.05	−8.980	−29.800

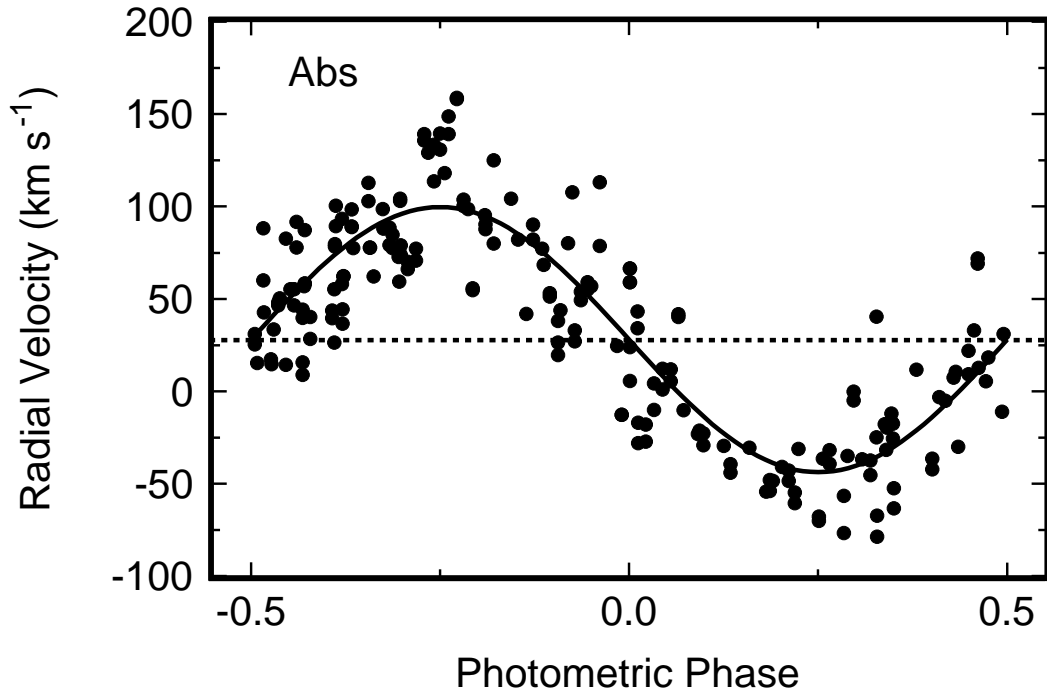


Fig. 1.— Absorption line radial velocity curve. The solid line is the best-fitting circular orbit to the measured velocities (filled circles). The dashed line indicates the systemic velocity.

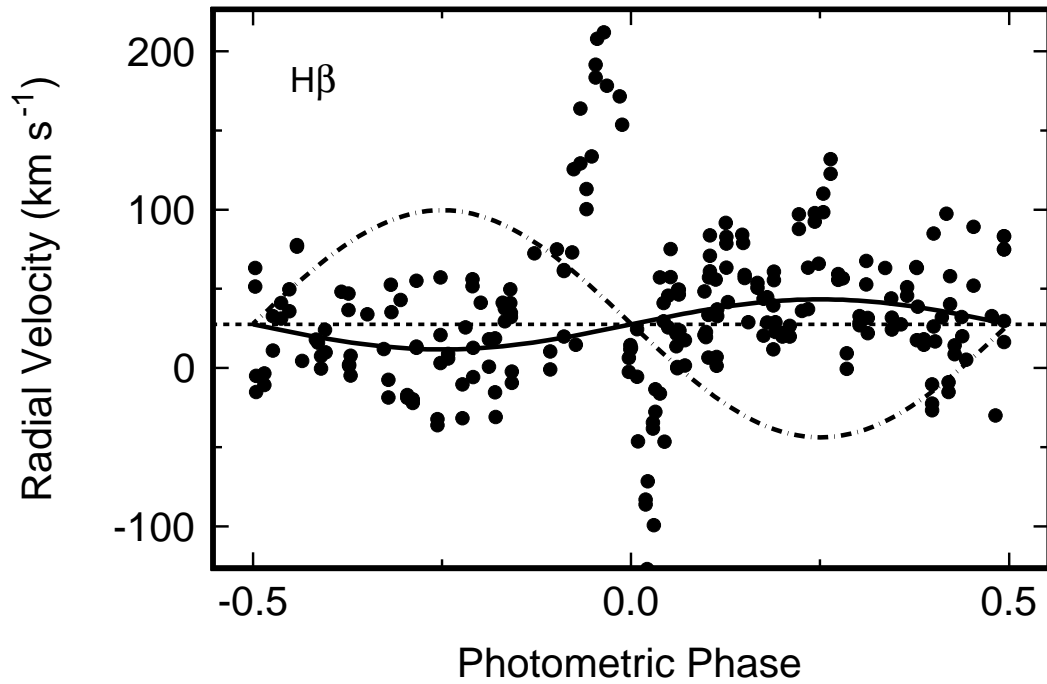


Fig. 2.— Emission line radial velocity data for H β . The dot-dashed curve repeats the absorption line orbit from Figure 1; the dashed line indicates the systemic velocity derived from the absorption line orbit. The solid line is the orbit inferred from the H β velocities outside of primary eclipse ($\phi = 0.05$ – 0.95).

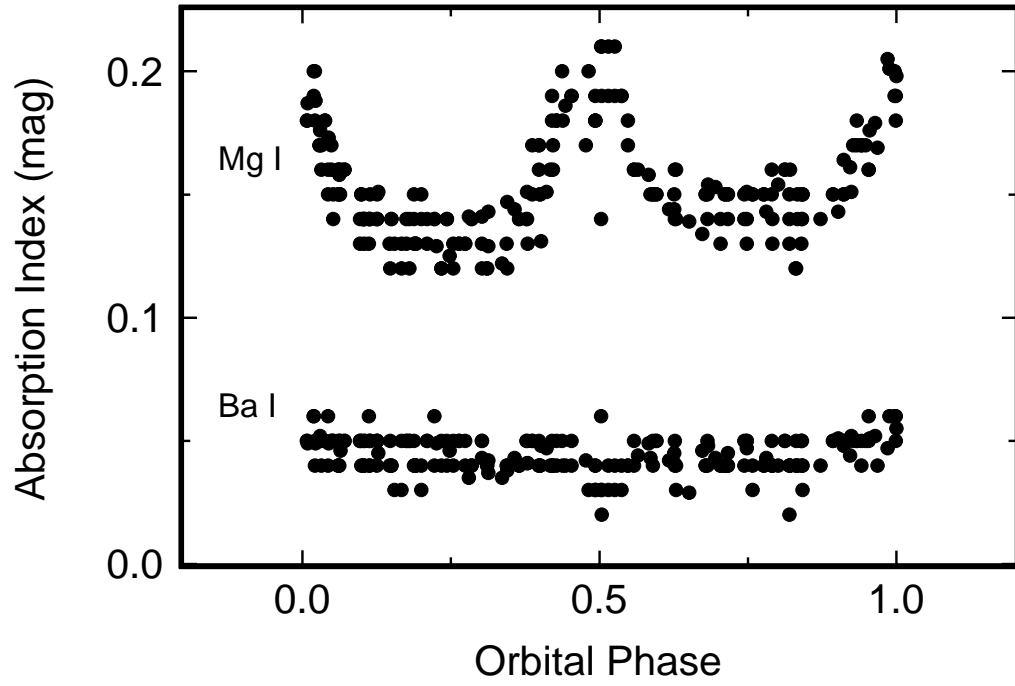


Fig. 3.— Variation of absorption line indices. The Ba I index at 6495 \AA is nearly constant with phase. The Mg I index strengthens during primary eclipse and during secondary eclipse.

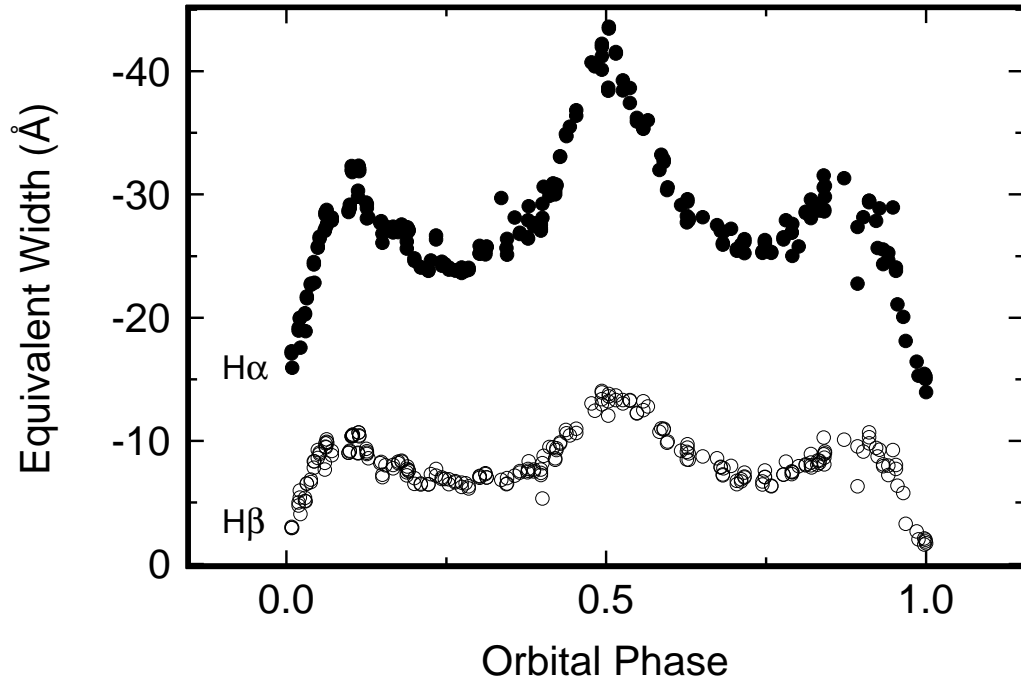


Fig. 4.— Variation of emission line equivalent widths. The H I emission is eclipsed by the secondary at $\phi = 0$. Because the continuum declines when the disk eclipses the K0 I secondary star, the equivalent widths rise at $\phi = 0.5$. Outside of eclipse, the equivalent widths vary sinusoidally in phase with the ellipsoidal variations of the secondary.